IEEE Industrial Electronics Society. University of Zagreb. IEEE Hungary Section. Budapest Polytechnic, Hungary. Hungarian Fuzzy Association.

2002 International Conference

on Intelligent Engineering Systems

IEEE Networking the World ™

INES 2002

Opatija, Croatia May 26-28

Proceedings

Application of Fractional Calculus in the Control of Mechanical Systems

J. A. Tenreiro Machado
Dept. of Electrical Eng.
Institute of Engineering
4200-072 Porto
Portugal
jtm@dee.isep.ipp.pt

Ramiro S. Barbosa
Dept. of Electrical Eng.
Institute of Engineering
4200-072 Porto
Portugal
rbarbosa@dee.isep.ipp.pt

Fernando B. M. Duarte
Dept. of Mathematics
Scholl of Technology
3504-510 Viseu
Portugal
fduarte@mat.estv.ipv.pt

Nuno M. F. Ferreira
Dept. of Electrical Eng.
Institute of Engineering
3031-601 Coimbra,
Portugal
nunomig@isec.pt

***Abstract* – The Fractional Calculus (FC) goes back to the beginning of the theory of differential calculus. Nevertheless, the application of FC just emerged in the last two decades, due to the progress in the area of chaos that revealed subtle relationships with the FC concepts. In the field of dynamical systems theory some work has been carried out but the proposed models and algorithms are still in a preliminary stage of establishment. Having these ideas in mind, the paper discusses a FC perspective in the study of the dynamics and control of mechanical systems.**

I. INTRODUCTION

The generalization of the concept of derivative $D^{\alpha}f(x)$ to non-integer values of α goes back to the beginning of the theory of differential calculus. In fact, Leibniz, in his correspondence with Bernoulli, L'Hôpital and Wallis (1695), had several notes about the calculation of $D^{1/2}f(x)$. Nevertheless, the development of the theory of Fractional Calculus (FC) is due to the contributions of many mathematicians such as Euler, Liouville, Riemann and Letnikov [1–3]. In the fields of physics [4] and chemistry, FC is presently associated with the modeling of electro-chemical reactions, irreversibility and electromagnetism [5–9]. The adoption of the FC in control algorithms has been recently studied [10–14] using the frequency and discrete-time domains. Nevertheless, this research is still giving its first steps and further investigation is required.

This article introduces the fundamental aspects of the theory of FC and presents novel results on the dynamics and control of mechanical systems [15]. In this perspective, the paper is organized as follows. Section II outlines the main mathematical aspects of the theory of FC. Section III introduces the main algorithms to approximate fractional-order derivatives. Section IV presents several case studies on the implementation of FC-based models in the analysis and control of mechanical systems. Finally, section V draws the main conclusions.

II. MAIN MATHEMATICAL ASPECTS OF THE THEORY OF FRACTIONAL CALCULUS

Since the foundation of the differential calculus the generalization of the concept of derivative and integral to a non-integer order α has been the subject of several approaches. Due to this reason there are various definitions of fractional-order integrals (Table I) which are proved to be equivalent.

Based on the proposed definitions it is possible to calculate the fractional-order integrals/derivatives of several functions (Table II). Nevertheless, the problem of devising and implementing fractional-order algorithms is not trivial and will be the matter of the next sections.

TABLE I

SOME DEFINITIONS OF FRACTIONAL-ORDER INTEGRALS

Riemann-Liouville	$\left(I_{a+}^{\alpha}\varphi\right)(x)=\frac{1}{\Gamma(\alpha)}\int_a^x\frac{\varphi(t)}{(x-t)^{1-\alpha}}dt,\ a<x$
	$\left(D_{a+}^{\alpha}\varphi\right)(x)=\frac{1}{\Gamma(1-\alpha)}\frac{d}{dx}\int_a^x\frac{\varphi(t)}{(x-t)^{\alpha}}dt,\ a<x$
Grünwald-Letnikov	$\left(I_{a+}^{\alpha}\varphi\right)(x)=\frac{1}{\Gamma(\alpha)}\lim_{h\to+0}\left[h^{\alpha}\sum_{j=0}^{[(x-a)/h]}\frac{\Gamma(\alpha+j)}{\Gamma(j+1)}\varphi(x-jh)\right]$
Laplace	$L\left\{I_{0+}^{\alpha}\varphi\right\}=L\{\varphi\}/s^{\alpha},\ \mathrm{Re}(\alpha)>0$
	$L\left\{D_{0+}^{\alpha}\varphi\right\}=s^{\alpha}L\{\varphi\},\ \mathrm{Re}(\alpha)\geq 0$

TABLE II

FRACTIONAL-ORDER INTEGRALS OF SEVERAL FUNCTIONS

$\varphi(x),\ x\in\Re$	$\left(I_{+}^{\alpha}\varphi\right)(x),\ x\in\Re,\ \alpha\in C$
$(x-a)^{\beta-1}$	$\frac{\Gamma(\beta)}{\Gamma(\alpha+\beta)}(x-a)^{\alpha+\beta-1},\ \mathrm{Re}(\beta)>0$
$e^{\lambda x}$	$\lambda^{-\alpha}e^{\lambda x},\ \mathrm{Re}(\lambda)>0$
$\begin{cases}\sin(\lambda x)\\ \cos(\lambda x)\end{cases}$	$\lambda^{-\alpha}\begin{cases}\sin(\lambda x-\alpha\pi/2)\\ \cos(\lambda x-\alpha\pi/2)\end{cases},\ \lambda>0,\mathrm{Re}(\alpha)>1$
$e^{\lambda x}\begin{cases}\sin(\gamma x)\\ \cos(\gamma x)\end{cases}$	$\frac{e^{\lambda x}}{(\lambda^2+\gamma^2)^{\alpha/2}}\begin{cases}\sin(\gamma x-\alpha\phi)\\ \cos(\gamma x-\alpha\phi)\end{cases},\ \phi=\arctan(\gamma/\lambda),\ \gamma>0,\mathrm{Re}(\lambda)>1$

III. APPROXIMATIONS TO FRACTIONAL-ORDER DERIVATIVES

In this section we analyze two methods for implementing fractional-order derivatives, namely the frequency-based and the discrete-time approaches, and its implication in control algorithms.

In order to analyze a frequency-based approach to D^{α}, $0<\alpha<1$, let us consider the recursive circuit represented on Fig. 1 such that:

$$I=\sum_{i=0}^{n}I_i,\ R_{i+1}=\frac{R_i}{\varepsilon},\ C_{i+1}=\frac{C_i}{\eta} \tag{1}$$

where η and ε are scale factors, I is the current due to an applied voltage V and R_i and C_i are the resistance and capacitance elements of the i^{th} branch of the circuit.

The admittance $Y(j\omega)$ is given by:

$$Y(j\omega)=\frac{I(j\omega)}{V(j\omega)}=\sum_{i=0}^{n}\frac{j\omega C\varepsilon^{i}}{j\omega CR+(\eta\varepsilon)^{i}} \tag{2}$$

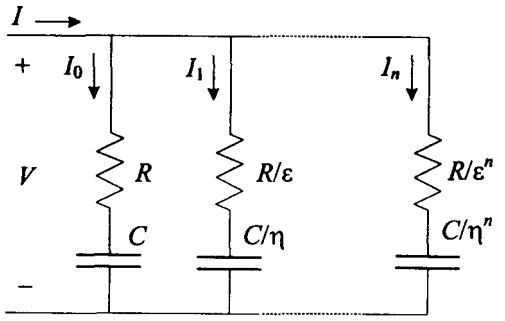

Fig. 1. Electrical circuit with a recursive association of resistance and capacitance elements

Fig. 2 shows the asymptotic Bode diagrams of amplitude and phase of $Y(j\omega)$. The pole and zero frequencies (ω_i and ω_i') obey the recursive relationships:

$$\frac{\omega_{i+1}'}{\omega_i'} = \frac{\omega_{i+1}}{\omega_i} = \varepsilon\eta\,,\ \frac{\omega_i}{\omega_i'} = \varepsilon\,,\ \frac{\omega_{i+1}'}{\omega_i} = \eta \tag{3}$$

From the Bode diagram of amplitude or of phase, the average slope m' can be calculated as:

$$m' = \frac{\log\varepsilon}{\log\varepsilon + \log\eta} \tag{4}$$

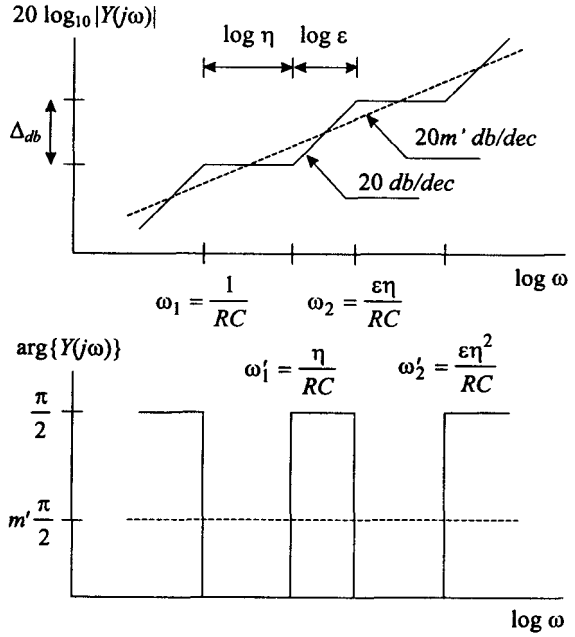

Fig. 2. Bode diagrams of amplitude and phase of $Y(j\omega)$

Consequently, the circuit of Fig. 1 represents an approach to D^α, $0 < \alpha < 1$, with $m' = \alpha$, based on a recursive pole/zero placement in the frequency domain.

As mentioned in section II, the Laplace definition for a derivative of order $\alpha \in C$ is a 'direct' generalization of the classical integer-order scheme with the multiplication of the signal transform by the s operator. Therefore, in what concerns automatic control theory this means that frequency-based analysis methods have a straightforward adaptation to their fractional-order counterparts. Nevertheless, the implementation based on the Laplace definition (adopting the frequency domain) requires an infinite number of poles and zeros obeying a recursive relationship [10–11]. In a real approximation the finite number of poles and zeros yields a ripple in the frequency response and a limited bandwidth.

Based on the Grünwald-Letnikov definition of a derivative of fractional order α of the signal $x(t)$, $D^\alpha x(t)$, leads to the expression:

$$D^\alpha x(t) = \lim_{h\to 0}\left[\frac{1}{h^\alpha}\sum_{k=0}^{\infty}(-1)^k\frac{\Gamma(\alpha+1)}{\Gamma(k+1)\Gamma(\alpha-k+1)}x(t-kh)\right] \tag{5}$$

where Γ is the gamma function and h is the time increment. This formulation [12–14] inspired a discrete-time calculation algorithm, based on the approximation of the time increment h through the sampling period T, yielding the equation in the z domain:

$$\frac{Z\{D^\alpha x(t)\}}{X(z)} \approx \frac{1}{T^\alpha}\sum_{k=0}^{\infty}\frac{(-1)^k\Gamma(\alpha+1)}{k!\,\Gamma(\alpha-k+1)}z^{-k} = \left(\frac{1-z^{-1}}{T}\right)^\alpha \tag{6}$$

An implementation of (6) corresponds to a r-term truncated series given by:

$$\frac{Z\{D^\alpha x(t)\}}{X(z)} \approx \frac{1}{T^\alpha}\sum_{k=0}^{r}\frac{(-1)^k\Gamma(\alpha+1)}{k!\,\Gamma(\alpha-k+1)}z^{-k} \tag{7}$$

Clearly, in order to have good approximations, we must have a large r and a small T.

An important aspect of fractional-order controllers can be illustrated through the elemental control system represented in Fig. 3, with open-loop transfer function $G(s) = Ks^{-\alpha}$ ($1 < \alpha < 2$) in the forward path. The open-loop Bode diagrams (Fig. 4) of amplitude and phase have a slope of -20α *dB/dec* and a constant phase of $-\alpha\pi/2$ *rad*, respectively. Therefore, the closed-loop system has a constant phase margin of $\pi(1-\alpha/2)$ *rad*, that is independent of the system gain K.

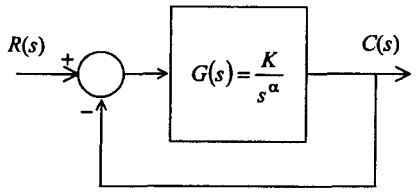

Fig. 3. Block diagram for an elemental feedback control system of fractional order α

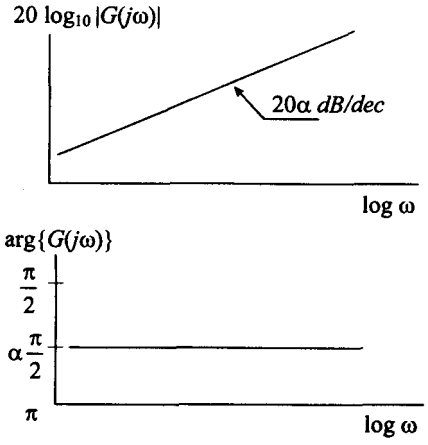

Fig. 4. Open-loop Bode diagrams of amplitude and phase for a system of fractional order $1 < \alpha < 2$

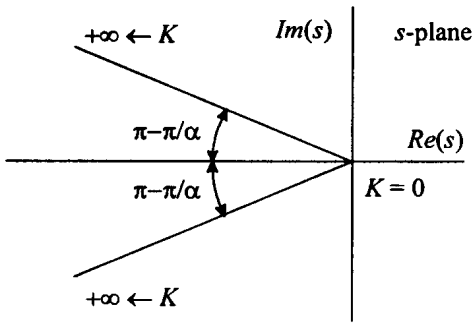

Fig. 5. Root locus for a feedback control system of fractional order $1 < \alpha < 2$

Likewise, this important property is also revealed through the root-locus depicted in Fig. 5.

IV. CONTROL OF MECHANICAL SYSTEMS

In this section we study the adoption of fractional-order algorithms in the dynamics and control of mechanical systems.

A. Describing Function of Systems with Backlash

The standard approach to the backlash study is based on the adoption of a geometric model that neglects the dynamic phenomena involved during the impact process. Due to this reason often real results differ significantly from those predicted by that model. In this section, we use the describing function (DF) method to analyse systems with backlash and impact phenomena, usually called *dynamic backlash*.

The proposed mechanical model consists on two masses (M_1 and M_2) with backlash and impacts as shown in Fig. 6.

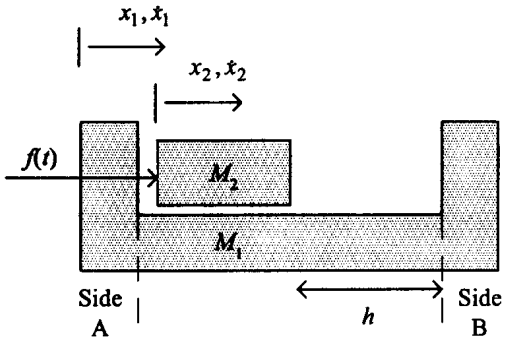

Fig. 6. System with two masses subjected to dynamic backlash

A collision between the masses M_1 and M_2 occurs when $x_1 = x_2$ or $x_2 = h + x_1$. In this case, we can compute the velocities of masses M_1 and M_2 after the impact ($\dot{x}_1'$ and $\dot{x}_2'$) by relating them to the previous values ($\dot{x}_1$ and $\dot{x}_2$) through Newton's law:

$$(\dot{x}_1' - \dot{x}_2') = -\varepsilon\,(\dot{x}_1 - \dot{x}_2), \quad 0 \le \varepsilon \le 1 \tag{8}$$

where ε is the coefficient of restitution. In the case of a fully plastic (*inelastic*) collision $\varepsilon = 0$, while in the *ideal elastic* case $\varepsilon = 1$.

By application of the principle of conservation of momentum and of expression (8), we can find the sought velocities of both masses after an impact:

$$\dot{x}_1' = \frac{\dot{x}_1(M_1 - \varepsilon M_2) + \dot{x}_2(1+\varepsilon)M_2}{M_1 + M_2} \tag{9a}$$

$$\dot{x}_2' = \frac{\dot{x}_1(1+\varepsilon)M_1 + \dot{x}_2(M_2 - \varepsilon M_1)}{M_1 + M_2} \tag{9b}$$

We can calculate numerically the Nyquist diagram of $-1/N(F,\omega)$ for an input force $f(t) = F\cos(\omega t)$ applied to mass M_2 and an output position $x_1(t)$ of mass M_1.

Figs. 7–8 show the Nyquist plots for $F = 50$ N and $\varepsilon = \{0.1,\ldots,0.9\}$ and for $F = \{10, 20, 30, 40, 50\}$ N and $\varepsilon = 0.5$, respectively, considering $M_1 = M_2 = 1$ kg and $h = 10^{-1}$ m. The charts reveal the occurrence of a jumping phenomenon, which is a characteristic of nonlinear systems. This phenomenon is more visible around $\varepsilon \approx 0.5$, while for the limiting cases ($\varepsilon \to 0$ and $\varepsilon \to 1$) the singularity disappears. Moreover, Fig. 8 shows also that for a fixed value of ε the charts are proportional to the input amplitude F.

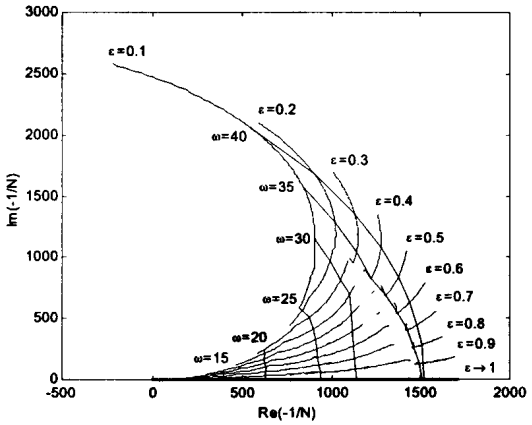

Fig. 7. Nyquist plot of $-1/N(F,\omega)$ for the dynamic backlash, $F = 50$ N and $\varepsilon = \{0.1, \ldots, 0.9\}$

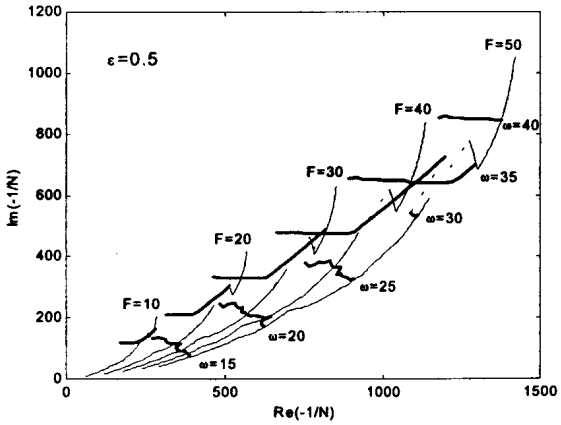

Fig. 8. Nyquist plot of $-1/N(F,\omega)$ for a system with dynamic backlash, $F = \{10, 20, 30, 40, 50\}$ N and $\varepsilon = 0.5$

The validity of the model is restricted to an input force $f(t)$ with frequency higher than a lower-limit $\omega_C \approx [(2F/M_2h)^2(1-\varepsilon)^5]^{1/4}$ and lower than an upper-limit $\omega_L = 2(F/M_2h)^{1/2}$, corresponding to an amplitude of $x_1(t)$ within the clearance $h/2$. In the middle-range occurs a jumping phenomena at frequency $\omega_J \sim (F/M_2h)^{1/2}$.

Fig. 9 shows the log-log plots of Re{−1/N} and Im{−1/N} *vs.* ω with $F = 50$ N and $\varepsilon = \{0.1, 0.3, 0.5, 0.7, 0.9\}$, for the cases of the static and dynamic backlash.

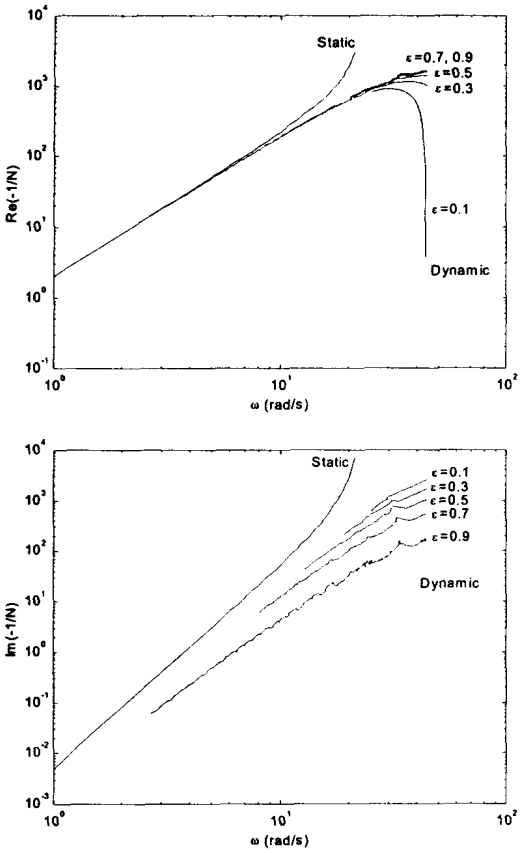

Fig. 9. Log-log plots of Re{−1/N} and Im{−1/N} vs. the exciting frequency ω, for F = 50 N and ε = {0.1, 0.3, 0.5, 0.7, 0.9}

The classical static backlash model corresponds to the DF of a linear system of a single mass M_1+M_2 followed by the geometric backlash having as input and as output the position variables. Comparing the results for the static and the dynamic backlash models we conclude that:

- The charts of Re{−1/N}are similar for low frequencies (where they reveal a slope of +40 dB/dec) but differ significantly for high frequencies;
- The charts of Im{−1/N} are different in all range of frequencies. Moreover, for low frequencies, the dynamic backlash has a fractional slope inferior to +80 dB/dec of the static model.

A careful analysis must be taken because it was not demonstrated that a DF fractional slope would imply a fractional-order model. In fact, in this study we adopt integer-order models for the system description but the fractional-order slope is due to continuous/discrete dynamic variation that results due to the mass collisions.

B. Trajectory Control of Redundant Manipulators

A redundant manipulator possess more degrees-of-freedom (*dof*) than those required to establish an arbitrary position and orientation of the gripper (Fig. 10). We consider a manipulator with *n dof* whose joint variables are denoted by $\mathbf{q} = [q_1,q_2,...,q_n]^T$ and a class of operational tasks described by *m* variables $\mathbf{x} = [x_1,x_2,...,x_m]^T$, $m < n$. The relation between the joint vector **q** and the manipulation vector **x** corresponds to the direct kinematics:

$$\mathbf{x} = f(\mathbf{q}) \tag{10}$$

Differentiating (10) with respect to time yields:

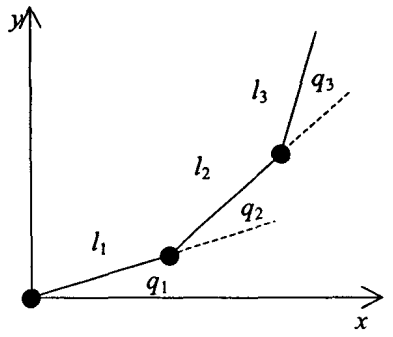

Fig. 10. The 3*R* planar redundant manipulator

$$\dot{\mathbf{x}} = \mathbf{J}(\mathbf{q})\dot{\mathbf{q}} \tag{11}$$

Hence, from (11) it is possible to calculate a $\mathbf{q}(t)$ path in terms of a prescribed trajectory $\mathbf{x}(t)$. A solution is:

$$\dot{\mathbf{q}} = \mathbf{J}^{\#}(\mathbf{q})\dot{\mathbf{x}} \tag{12}$$

where $\mathbf{J}^{\#}$ is one of the generalized inverses of the **J**. The joint positions can be computed through the time integration of the velocities (12) according with the block diagram depicted in Fig. 11.

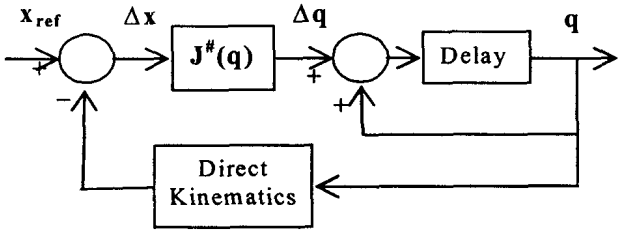

Fig. 11. Diagram of the closed-loop inverse kinematics algorithm with $\mathbf{J}^{\#}$

An important aspect is that repetitive trajectories in the operational space do not lead to periodic trajectories in the joint space. This is an obstacle for the solution of many tasks because the resultant robot configurations have similarities with those of a chaotic system.

We consider a 3*R* planar manipulator and during the experiments it is adopted $\Delta t = 10^{-3}$ s and $l_1 = l_2 = l_3 = 1$ m.

Fig. 12 depicts the 3*R*-robot phase-plane joint trajectories, when repeating a circular motion with frequency $\omega_0 = 3$ *rad/s*, center at $r = [x^2+y^2]^{1/2} = 1$ *m* and radius $\rho = 0.1$ *m*. Besides the position and velocity drifts, leading to different trajectory loops, we have points that are 'avoided'. Such points correspond to arm configurations where several links are aligned.

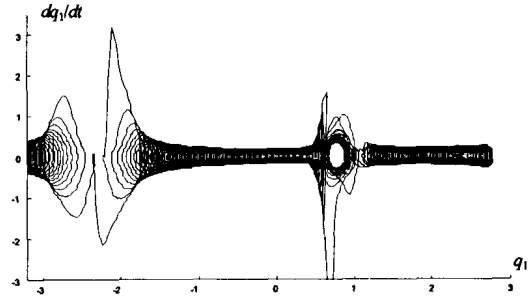

Fig. 12. Phase plane trajectory for the 3*R*- robot joint 1 at $r = 1$ m, $\rho = 0.1$ m, $\omega_0 = 3$ rad/s

In order to capture information about the system during all the dynamic evolution we devised an experiment that addresses the frequency response for two alternative exciting signals: a doublet-like and a white noise distributed throughout the 500-cycle trajectories. Fig. 13 depicts the resulting amplitude Bode diagrams of the type:

$$Q_1(s)/X_{ref}(s) = K\left(s^{\alpha} + z\right)/\left(s^{\alpha} + p\right) \qquad (13)$$

where K is the gain, z and p are the zero and pole, respectively, and α is the zero/pole fractional-order.

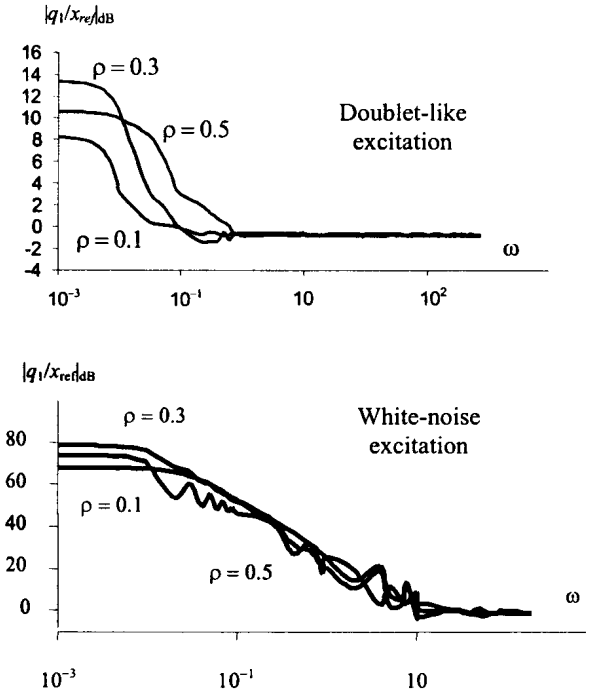

Fig. 13. Frequency response of the 3R robot $\omega_0 = 3$ rad/s, $r = 2$ m, $\rho \in \{0.10, 0.30, 0.50\}$ m for: a doublet-like and a white noise perturbation during all trajectory

For the doublet excitation it results $\alpha \approx 1.0$ in contrast with the case of white noise excitation where we get a fractional value $\alpha \approx 1.3$. This is due to the memory-time property of fractional-order dynamics because they capture the dynamic phenomena involved during all the time-history of the experiment, in contrast with integer-order derivative that just capture a "local" dynamics.

In a different experiment we calculate the Fourier transform of the robot joint velocities for a large number of cycles of circular repetitive motion with frequency ω_0. Fig. 14 shows the results for the 3R robot *vs.* the radial distance r, for a circle with radius ρ. We verify that for $0 < r < 1$ we get a chaotic behaviour with a signal energy distribution along all frequencies, while for $1 < r < 3$ m the signal energy is concentrated at the fundamental and multiple harmonics.

C. Position/force Control of Manipulators

This section studies the position/force robot control, involving contact between the gripper and the environment, using fractional-order controllers in the hybrid algorithm proposed by Raibert and Craig [15].

The dynamical equation of a robot with n links interacting with the environment (Fig. 15) is given by:

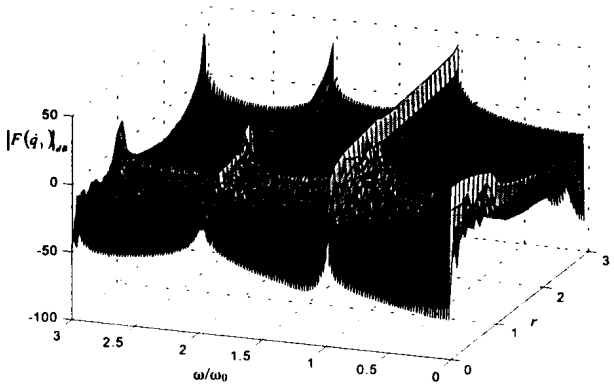

Fig. 14. Fourier transform of dq_1/dt, for 500 cycles, *vs.* the radial distance r and the frequency ratio ω/ω_0, for $\rho = 0.1$ *m*, $\omega_0 = 3$ *rad/s*

$$\boldsymbol{\tau} = \mathbf{H}(\mathbf{q})\ddot{\mathbf{q}} + \mathbf{C}(\mathbf{q},\dot{\mathbf{q}}) + \mathbf{G}(\mathbf{q}) - \mathbf{J}^{\mathrm{T}}(\mathbf{q})\mathbf{F} \qquad (14)$$

where $\boldsymbol{\tau}$ and $\mathbf{q}$ are the $n \times 1$ vectors of joint torques and positions, $\mathbf{H}(\mathbf{q})$ is the $n \times n$ inertia matrix, $\mathbf{C}(\mathbf{q},\dot{\mathbf{q}})$ and $\mathbf{G}(\mathbf{q})$ are the $n \times 1$ vectors of centrifugal/Coriolis and gravitational terms and $\mathbf{F}$ is the $m \times 1$ vector of the force that the environment exerts in the robot gripper.

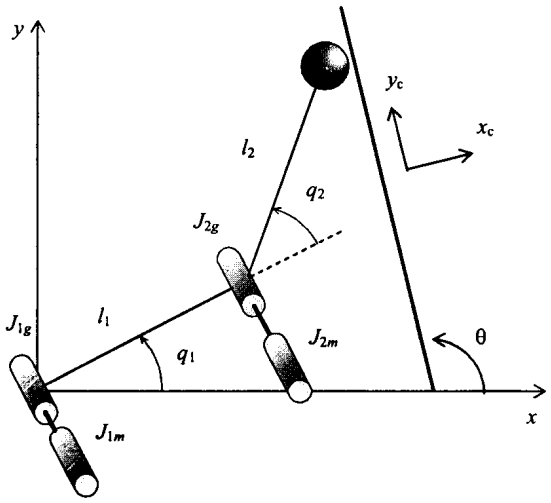

Fig. 15. The 2R robot and the constraint surface

We adopt the 2R robot and for joint gear i ($i = 1,2$) we consider a clearance h_i and impact phenomena between the inertias, obeying formulae (9). The contact displacement x_C of the gripper with the surface is modeled through a system with a mass M, a damping B and a stiffness K.

The schematic structure of the position/force hybrid control algorithm is depicted in Fig. 16. The diagonal $n \times n$ selection matrix $\mathbf{S}$ has elements equal to one (zero) in the position (force) controlled directions and $\mathbf{I}$ is the $n \times n$ identity matrix. In this paper we consider the y_C (x_C) Cartesian coordinates to be position (force) controlled.

For the position and force controllers we adopt fractional-order algorithms based on scheme (7). Moreover, in the experiments, we study the system time response for $\theta = \pi/2$ and the initial operating point $q_{10} = q_{20} = 15\pi/36$, where q_{i0} stands for the initial position for the joint i. At $t = 0.1$ s it is applied a step at the force reference of $F_d = 1$ N and a zero increment at the position input $y_{cd} = y_{c0}$. The numerical values adopted for the 2R

robot are $m_1 = 0.5$ kg, $m_2 = 6.25$ kg, $r_1 = 1.0$ m, $r_2 = 0.8$ m, $J_{im} = 1.0$ Kgm^2 and $J_{ig} = 4.0$ Kgm^2 ($i = 1,2$). The parameters for the constraint surface and for the backlash are $M = 0.03$ kg, $B = 1$ Ns/m and $K = 400$ N/m are $h_i = 0.00018$ rad and $\varepsilon_i = 0.5$ ($i = 1,2$), respectively.

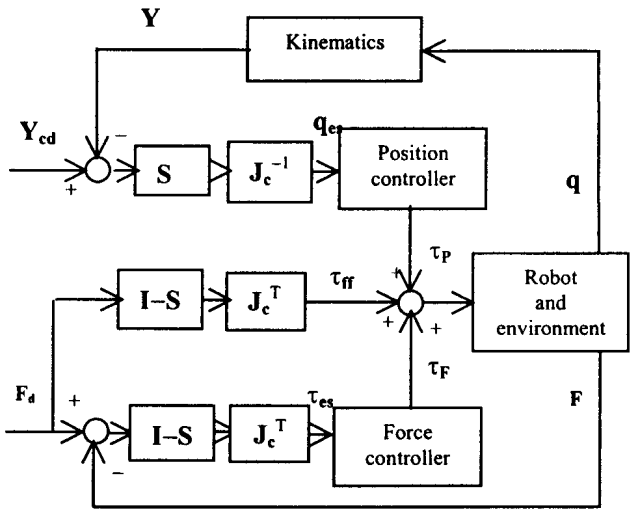

Fig. 16. The position/force hybrid controller

The fractional-order controllers were tuned by trial and error (with a compromise between fast transients and large overshoots) leading to $K_{Pi} = 5000$, $K_{Fi} = 50$, $\alpha_{Pi} = 1/2$, $\alpha_{Fi} = 1/5$ and $r_{Pi} = r_{Fi} = 17$ ($i = 1,2$). Each controller gain is denoted by K, the subscripts P or F stand for the position or force loops and the sampling frequency is $f_c = 1$ kHz.

The results (Fig. 17) revealed that the fractional-order algorithms have a very good performance, difficult to get with classical control algorithms.

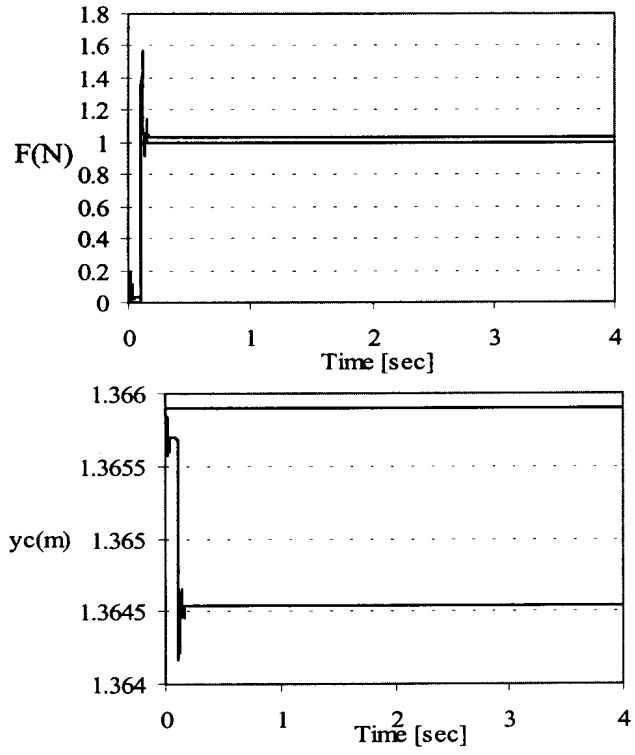

Fig. 17. Time response for the 2*R* robot with backlash

V. CONCLUSIONS

This paper presented the fundamental aspects of the FC calculus, the main approximation methods for the fractional-order derivatives calculation and the implication of the FC concepts on the extension of the classical automatic control theory. Bearing these ideas in mind, several motion control systems were described and their dynamics was analyzed in the perspective of fractional calculus. It was shown that fractional-order models capture phenomena and properties that classical integer-order simply neglect. In this line of thought, this article is a step towards the development of motion control systems based on the theory of FC.

VI. REFERENCES

[1] K. B. Oldham and J. Spanier, *The Fractional Calculus*. Academic Press, 1974.

[2] S. G. Samko, A. A. Kilbas, O. I. Marichev, *Fractional Integrals and Derivatives*, Gordon and Breach Science Publishers, 1993.

[3] K. S. Miller and B. Ross, *An Introduction to the Fractional Calculus and Fractional Differential Equations*, John Wiley and Sons, 1993.

[4] R. Hilfer, *Applications of Fractional Calculus in Physics*, World Scientific, Singapore: 2000.

[5] R. C. Koeller, "Applications of Fractional Calculus to the Theory of Viscoelasticity," *ASME Journal of Applied Mechanics*, vol. 51, June 1984, pp. 299–307.

[6] P. J. Torvik and R. L. Bagley, "On the Appearance of the Fractional Derivative in the Behaviour of Real Materials," *ASME Journal of Applied Mechanics*, vol. 51, June 1984, pp. 294–298.

[7] Åsa Fenander, "Modal Synthesis when Modeling Damping by Use of Fractional Derivatives," *AIAA Journal*, vol. 34, no. 5, May 1996, pp. 1051–1058.

[8] T. J. Anastasio, "The Fractional-Order Dynamics of Brainstem Vestibulo-oculomotor Neurons," *Biological Cybernetics*, vol. 72, 1994, pp. 69–79.

[9] H. M. Ozaktas, O. Arikan, M. A. Kutay and G. Bozdagi, "Digital Computation of the Fractional Fourier Transform," *IEEE Transactions on Signal Processing*, vol. 44, no. 9, Sept. 1996, pp. 2141–2150.

[10] A. Oustaloup, *La Commande CRONE: Commande Robuste d'Ordre Non Entier*, Hermes, Paris: 1991.

[11] A. Oustaloup, *La Dérivation Non Entière: Théorie, Synthèse et Applications*, Hermes, Paris: 1995.

[12] J. T. Machado, "Discrete-Time Fractional-Order Controllers," *FCAA Fractional Calculus and Applied Analysis*, vol. 4, no. 1, 2001, pp. 47–66.

[13] J. T. Machado, "Analysis and Design of Fractional-Order Digital Control Systems," *SAMS Journal Systems Analysis, Modelling, Simulation*, vol. 27, 1997, pp. 107–122.

[14] I. Podlubny, *Fractional Differential Equations*, Academic Press, San Diego: 1999.

[15] M. Raibert and J. Craig, "Hybrid Position/Force Control of Manipulators," ASME Journal of Dynamic Systems, Measurement, and Control, vol. 102, no. 2, 1981, pp. 126–133.